AD-A109 874 UTAH UNIV SALT LAKE CITY DEPT OF METEOROLOGY F/G 4/2
INVESTIGATION OF THE FORWARD RADIATIVE TRANSFER PROBLEM UTILIZI--ETC(U)
SEP 80 K LIOU, G C AUFDERHAAR, K HUTCHISON F19628-80-C-0108
UNCLASSIFIED AFGL-TR-80-0339 NL

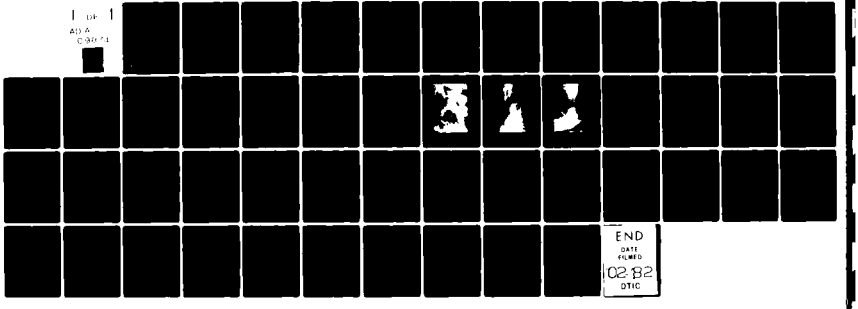

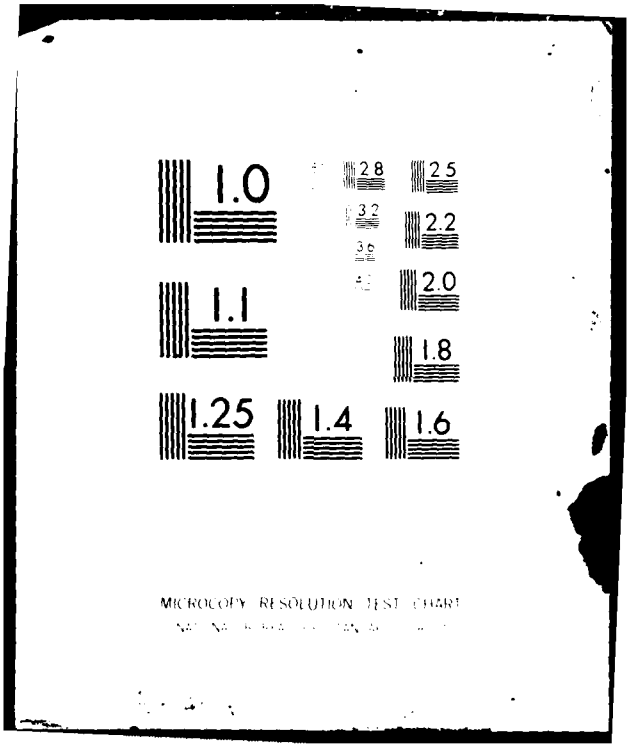
1.0
2.8
2.5
3.2
2.2
3.6
2.0
1.1
1.8
1.25
1.4
1.6
MICROCOPY RESOLUTION TEST CHART

AFGL-TR-80-0339

LEVEL II 12

INVESTIGATION OF THE FORWARD RADIATIVE TRANSFER PROBLEM UTILIZING DMSP AND NIMBUS 6 DATA

by

Kuo-Nan Liou, Grant C. Aufderhaar, Keith Hutchison
and Hwa-Young Yeh

Department of Meteorology
University of Utah
Salt Lake City, Utah 84112

30 September 1980

Final Report for Period
1 April 1980 to 30 September 1980

Approved for public release; distribution unlimited

AIR FORCE GEOPHYSICS LABORATORY
AIR FORCE SYSTEMS COMMAND
UNITED STATES AIR FORCE
HANSCOM AFB, MASSACHUSETTS 01731

Unclassified

SECURITY CLASSIFICATION OF THIS PAGE (When Data Entered)

REPORT DOCUMENTATION PAGE	READ INSTRUCTIONS BEFORE COMPLETING FORM
1. REPORT NUMBER: AFGL-TR-80-0339	2. GOVT ACCESSION NO.: AD A109874
3. RECIPIENT'S CATALOG NUMBER	
4. TITLE (and Subtitle): Investigation of the Forward Radiative Transfer Problem Utilizing DMSP and Nimbus 6 Data	5. TYPE OF REPORT & PERIOD COVERED: Final Report 4/1/80 - 9/30/80
	6. PERFORMING ORG. REPORT NUMBER
7. AUTHOR(s): Kuo-Nan Liou, Grant C. Aufderhaar, Keith Hutchison, Hwa-Young Yeh	8. CONTRACT OR GRANT NUMBER(s): F19628-80-C-0108 (changed to F19628-81-K-0019)
9. PERFORMING ORGANIZATION NAME AND ADDRESS: Department of Meteorology, University of Utah, Salt Lake City, Utah 84112	10. PROGRAM ELEMENT, PROJECT, TASK AREA & WORK UNIT NUMBERS: 62101F, 767013AA
11. CONTROLLING OFFICE NAME AND ADDRESS: Air Force Geophysics Laboratory, Hanscom AFB, Massachusetts 01731, Contract Monitor: Vincent Falcone/LYS	12. REPORT DATE: 30 September 1980
	13. NUMBER OF PAGES: 50
14. MONITORING AGENCY NAME & ADDRESS (if different from Controlling Office)	15. SECURITY CLASS. (of this report): Unclassified
	15a. DECLASSIFICATION DOWNGRADING SCHEDULE

16. DISTRIBUTION STATEMENT (of this Report)

Approved for public release; distribution unlimited.

17. DISTRIBUTION STATEMENT (of the abstract entered in Block 20, if different from Report)

18. SUPPLEMENTARY NOTES

19. KEY WORDS (Continue on reverse side if necessary and identify by block number)

Radiative Transfer	DMSP Block 5D Satellite	Nimbus 6 Satellite
Infrared Radiation	SSH Sounder	HIRS
Microwave Radiation	SSM/T Sounder	SCAMS
Rempte Sensing	Data comparison	

20. ABSTRACT (Continue on reverse side if necessary and identify by block number)

Comparison programs involving the computed radiances and brightness temperatures, utilizing the measured temperature and mixing ratio profiles from radiosonde, and the colocated observed data are carried out for the DMSP SSH (infrared) and SSM/T (microwave) sounders. In addition, a parallel comparison program using the Nimbus 6 HIRS and SCAMS data also is performed independently to examine the probable discrepancies between computations based on the conventional transfer equation and satellite observations. Appreciable

DD FORM 1 JAN 73 1473

Unclassified

SECURITY CLASSIFICATION OF THIS PAGE (When Data Entered)

20. (cont.)
discrepancies between computations and observations are shown for the SSH 15 μm CO_2 temperature channels whose weighting functions peak below about 16 km. These discrepancies also are supported by the comparison results from the Nimbus 6 HIRS 15 μm CO_2 channels and to a limited extent the DMSP SSM/T microwave sounders. It is found that computations generally exceed the observed radiances. In view of these finds, there appears to be definitive differences between the computations by means of the conventional radiative transfer solution and observed radiances, at least in the infrared CO_2 frequencies. Following these investigations, we recommend that a carefully designed field experiment, involving simultaneous and colocated infrared radiance observations in the 15 μm CO_2 frequencies and temperature and mixing ratio measurements, be carried out to further examine the quantitative validity of the conventional radiative transfer solution which has been fundamental to the sounding of the temperature profile from orbiting meteorological satellites.

TABLE OF CONTENTS

ACKNOWLEDGMENTS

We would like to thank Vince Falcone and Tony D'Agati for providing the needed transmittance routines for the DMSP SSH and SSM/T channels and for many helpful discussions. We also would like to extend our appreciation to Dr. Jean F. King for his constant encouragement in our research work sponsored by the Air Force Geophysics Laboratory. The cooperation of Captain Joseph Gahlingher of the Air Force Global Weather Central for providing the timely DMSP data is gratefully appreciated. We also thank the Ogden Air Logistics Center, Data Automation Branch, Comptroller at Hill Air Force Base, Utah, for providing computer time used in this investigation. The research work reported here was supported by the Air Force Geophysics Laboratory, Air Force Systems Command, under Contract F19628-80-C-0108. (Changed to F19628-81-K-0019)

Section 1

INTRODUCTORY REMARKS

In recent years, considerable progress has been achieved on the development of sounding techniques and theoretical and numerical fundamentals for the temperature and relevant gaseous retrieval in the earth's atmosphere. However, the success and reliability of the temperature field inverted from the sounding data, which are derived from orbiting meteorological satellites, have been long debated even in the limitation of clear atmosphere conditions.

Clearly, in order to perform a proper and reliable inversion program, it is essential that the forward problem based on the theoretical radiative transfer calculation be understood physically and numerically. In particular, we must understand the atmospheric and surface conditions under which the simulated radiances, derived from the conventional transfer theory, would match the observed values within the accuracy of the observation. For this purpose, we have carried out a comparison program for the observed and calculated radiances and brightness temperatures utilizing the available DMSP and Nimbus 6 data and the associated radiosonde and surface weather reports. We have restricted our comparison program to clear cases so that additional radiative complications due to multiple scattering of cloud and precipitation particles may be avoided. Moreover, we have focused our research effort on the infrared and microwave sounders aboard the Air Force Defense Meteorological Satellite Program (DMSP)

Block 5D Satellite System launched in June, 1979. These sounders are intended to provide data, on an operational mode, for deriving global basis temperature profiles in the troposphere and lower stratosphere.

In the course of intercomparisons between the simulated radiances obtained from radiative transfer theories and the measured DMSP and Nimbus 6 data, it is our objectives (1) to understand physical reasons for the possible significant uncertainties in the calculated radiances, (2) to examine the atmospheric and surface parameters under which these uncertainties arise, and (3) to investigate the validity of the simple transfer equation under restricted conditions (clear, known surface properties and temperature profiles, etc.). In connection with these studies, it is also necessary to examine and investigate the reliability and validity of the sounding data. In Section 2 of this report, we document the characteristics of DMSP SSH and SSM/T sounders and present results of the comparison for the computed and observed radiances from a set of carefully selected cases. Comparison programs utilizing the Nimbus 6 HIRS and SCAMS data are further described in Section 3. Finally, conclusions of this investigation are given in Section 4.

Section 2

COMPARISONS BETWEEN OBSERVED DMSP DATA AND CALCULATED RADIANCES

2.1 DMSP Block 5D SSH Sounder

2.1.1 Characteristics of the SSH sounder

The SSH (also called H-pack) is a scanning infrared spectro-radiometer which was launched in June, 1979, in a sun-synchronous polar orbit, by the United States Air Force as part of the Defense Meteorological Satellite Program (DMSP) Block 5D package. Other equipment of meteorological interest on board the spacecraft include a passive microwave temperature sounder (to be described in Subsection 2.2.1) and visual and infrared imagery channels. A sketch of the approximate track of the current DMSP satellite over the United States is depicted in Fig. 1. The horizontal lines along the satellite track in this figure show the scan patterns of infrared and microwave sounders. The SSH has 17 spectral bands. Specifically, the serial number 005, which is used in this investigation, measures infrared radiance in eight narrow H_2O bands, six narrow CO_2 bands, one narrow window band, and one ozone band for a total of 16 bands (see Table 1). The SSH provides soundings of temperature and humidity and a single measurement of ozone for vertical and slant paths lying under and to the side of the sub-satellite track.

The SSH generates a spatial pattern across the satellite subtrack such that 25 areas (ground stations) in a scan width about

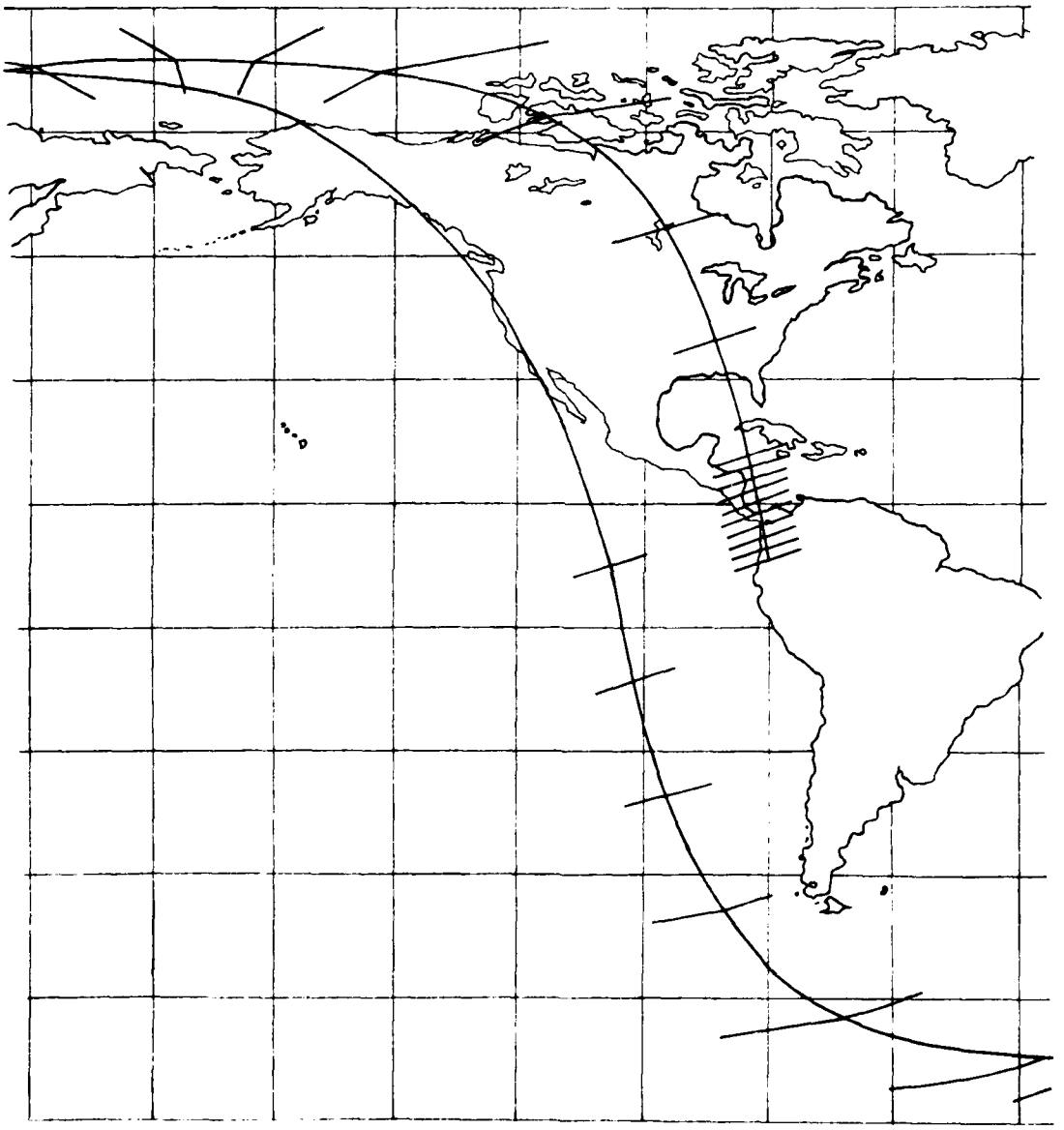

Fig. 1. The DMSP satellite track and scan patterns.

Table 1. SSH spectral band characteristics.

Wavelength μm	Wavenumber (cm^{-1})	Half width (cm^{-1})	Species
9.8	1022	12.5	O_3
12.0	835	8	window
13.4	747	10	CO_2
13.8	725	10	CO_2
14.1	708	10	CO_2
14.4	695	10	CO_2
14.8	676	10	CO_2
15.0	668.5	3.5	CO_2
18.7	535	16	H_2O
24.5	408.5	12	H_2O
22.7	441.5	18	H_2O
23.9	420	20	H_2O
26.7	374	12	H_2O
25.2	397.5	10	H_2O
28.2	355	15	H_2O
28.3	353.5	11	H_2O

1021 km on each side of nadir are spectrally interrogated once every 32 seconds. The scan pattern is accomplished by the use of a step-rotating scan mirror which completes one 360° rotation in a 32-second period. The ground look portion of the 32-second cycle occurs over the angular interval between +48° and -48° with 0° representing the nadir reference position. The 25 ground stations are measured at 4° at either side of nadir over this angular interval.

As shown in Fig. 2, the instantaneous field of view ground projection at the nadir position is a circle with a diameter of about 37 km. The ground projection at each successive station will evolve from a circle at nadir and become more noticeably elliptical at stations further away from nadir. At ±48° from nadir, the diameter of the field of view projection in the cross track direction is approximately 111 km, while the diameter in the long track direction is approximately 56 km. The ground projection centers shown in Fig. 2 represents the centroid rays at each ground station. The distance between each centroid ray ground projection in the long track direction is 208 km at nadir. The satellite altitude is 834 km and the subsatellite velocity is approximately 6.5 km/s. The cross-track spacing is 58 km at nadir increasing to 157 km at the oblique maximum. This spatial scan pattern makes it possible to provide complete global soundings on a daily basis.

For the spectral characteristics of SSH channels, the F channel bands lie in the H_2O region from 353 cm^{-1} to 535 cm^{-1} and E channel bands are in the CO_2 region from 668 cm^{-1} to 747 cm^{-1}. The window and O_3 bands are centered at 835 and 1022 cm^{-1}, respectively.

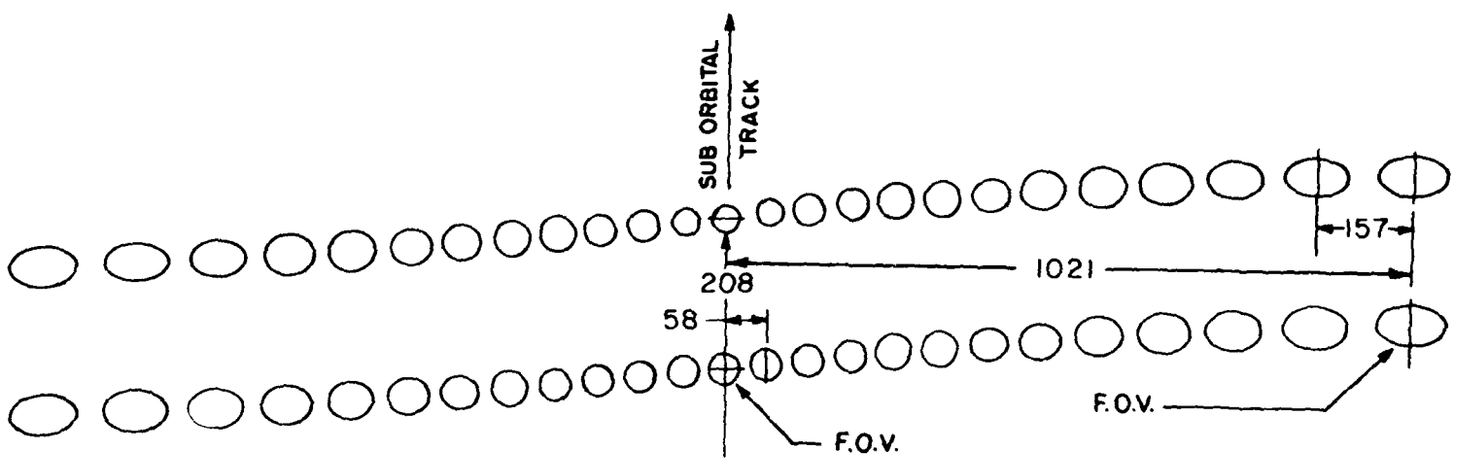

Fig. 2. DMSP Block 5D SSH scan patterns. F.O.V. stands for field of view. Distance Units are in km.

The filter data pertaining to the SSH sensor aboard the satellite used in this investigation can be found in the report prepared by Barnes Engineering Company for SAMSO (1976).

2.1.2 Comparisons between SSH data and calculated radiances

In this subsection we compare the observed data from SSH CO_2 channels and computed radiances utilizing the available radiosonde and synoptic data. We first describe the theoretical basis for the computation of infrared radiances and spectral transmittances for the CO_2 channels. We then discuss cases under which comparisons are made. Resulting comparisons are subsequently presented.

In the infrared region, under the condition of local thermodynamics equilbrium, the monochromatic upwelling radiance in pressure coordinates may be written as (see Liou, 1980)

$$I_\nu(o) = B_\nu(T_s)\,\tau_\nu(p_s) + \int_{p_s}^{o} B_\nu[T(p)]\,\frac{\partial \tau_\nu(p)}{\partial p}\,dp\ , \qquad (1)$$

where T_s and p_s are respectively the surface temperature and pressure, ν the wavenumber, B_ν the Planck function, and the monochromatic transmittance at the pressure level p is defined by

$$\tau_\nu(p) = \exp\left[-\frac{1}{g}\int_o^p q(p')k_\nu(p')dp'\right]\ , \qquad (2)$$

where g denotes the gravitational acceleration, q the mixing ratio, and k_ν the monochromatic absorption coefficient. However, an instrument, such as the SSH sensor, can only distinguish a finite band width $\phi(\bar{\nu},\nu)$, where ϕ and $\bar{\nu}$ denote the instrument response function and mean wavenumber of the band, respectively. Thus, the measured radiance from the spectrometer aboard the satellite over a wavenumber interval (ν_1,ν_2) in the normalized

form may then be expressed by

$$I_{\bar{\nu}}(o) = \int_{\nu_1}^{\nu_2} \phi(\bar{\nu},\nu)\ I_\nu d\nu \Big/ \int_{\nu_1}^{\nu_2} \phi(\bar{\nu},\nu) d\nu \tag{3}$$

Upon carrying out the wavenumber integration of Eq. (1), we obtain

$$I_{\bar{\nu}}(o) = \frac{1}{\int_{\nu_1}^{\nu_2} \phi(\bar{\nu},\nu) d\nu} \left[\int_{\nu_1}^{\nu_2} \phi(\bar{\nu},\nu)\ B_\nu(T_s) T_\nu(p_s) d\nu \right.$$

$$\left. + \int_{\nu_1}^{\nu_2} \phi(\bar{\nu},\nu) \int_{p_s}^{0} B_\nu\,[T(p)] \frac{\partial T_\nu(p)}{\partial p}\, dp\, d\nu \right]. \tag{4}$$

If the spectral interval (ν_1,ν_2) is small enough that the variation of $B_\nu(T)$ with respect to ν is insignificant so that its value may, to a good approximation, be replaced by $B_{\bar{\nu}}(T)$, then Eq. (4) becomes

$$I_{\bar{\nu}}(o) = B_{\bar{\nu}}(T_s)\ T_{\bar{\nu}}(p_s) + \int_{p_s}^{0} B_{\bar{\nu}}\,[T(p)] \frac{\partial T_{\bar{\nu}}(p)}{\partial p}\, dp\ , \tag{5}$$

where the spectral transmittance, when the instrument response function is taken into account, is defined by

$$T_{\bar{\nu}}(p) = \int_{\nu_1}^{\nu_2} \phi(\bar{\nu},\nu)\, T_\nu(p)\, d\nu \Big/ \int_{\nu_1}^{\nu_2} \phi(\bar{\nu},\nu) d\nu\ , \tag{6}$$

and the spectral weighting function is denoted as $\partial T_{\bar{\nu}}(p)/\partial p$.

Atmospheric transmittances for SSH CO_2 channels for selected cases were computed employing the transmittance program developed at the Air Force Geophysics Laboratory and provided to us. In the program, line-by-line calculations are performed using Eqs. (2) and (6) in which

the appropriate response function is taken into account for each channel. In the transmittance calculation for each case, temperature and mixing ratio profiles from radiosonde observations were used. Above about 10 mb if rocketsonde data were not available, then seasonally adjusted climatologies were used to extrapolate temperature, pressure, and mixing ratio to 40 pressure levels ranging from 1000 mb to 0.1 mb. The absorber concentration of water vapor (molecules/cm^2) was calculated as described by McClatchey et al. (1972) in conjunction with the AFGL transmittance program. A standard ozone profile was used for all cases.

Figures 3 and 4 depict for illustration purposes weighting function curves of six CO_2 channels for Winnemucca, Nevada (October 30, 1979) and Dodge City, Kansas (November 23, 1979), respectively. The peaks of these weighting functions indicate the approximate location in the atmosphere from which most of the energy that reaches the top of the atmosphere originates. The weighting function for each channel peaks at about the same height for these two stations. The maximum weighting function for channel E1 locates at about 4 and 30 mb. For channels E2, E3, and E4, weighting functions peak at about 85, 150, and 400 mb, respectively. Channels E5 and E6 are surface channels which sense the atmosphere near the earth's surface. The weighting functions of channels E5 and E6 for Winnemucca peak at 780 and 820 mb, respectively, while for Dodge City, they peak at 850 and 1000 mb, respectively. Clearly, the former weighting functions peak considerably higher than latter values, probably due to the altitude of Winnemucca (1,322 m) at which the surface pressure was reported to be 920 mb on this particular date.

We have selected two days, 30 October 1979, and 23 November 1979, during which complete data sets were available over the continental

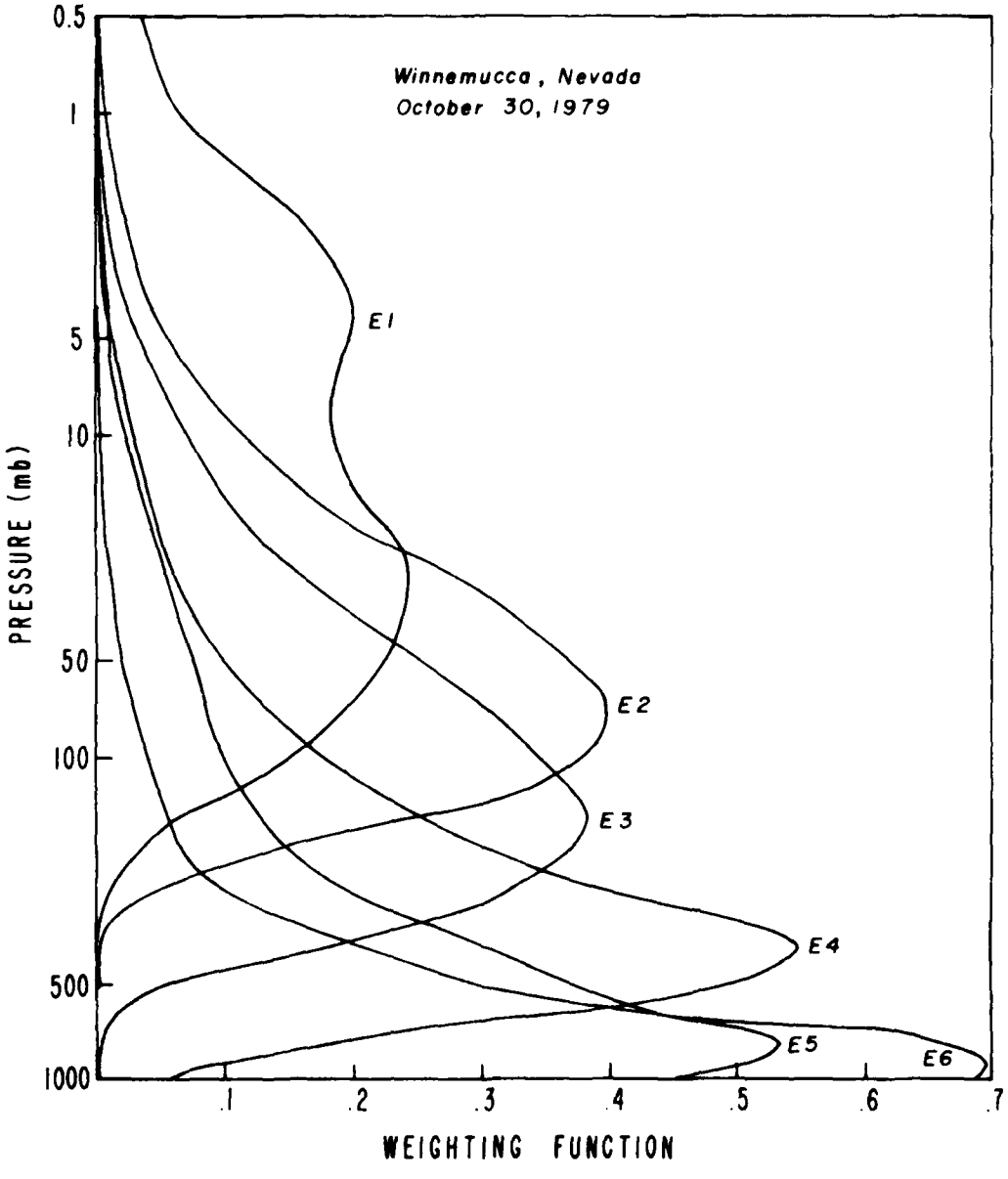

Fig. 3. Weighting functions of the SSH CO_2 channels for the station Winnemucca, Nevada on 30 October 1979.

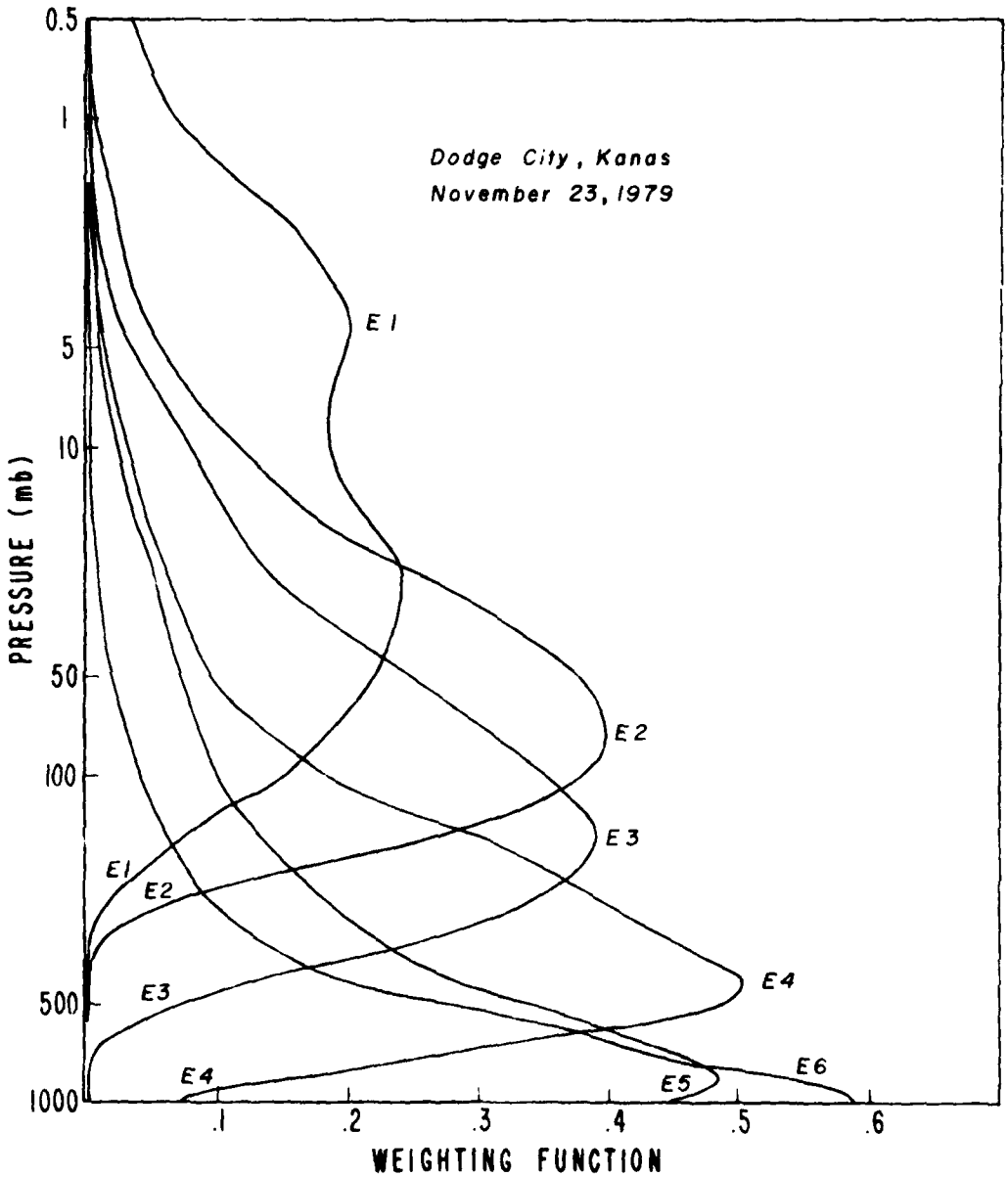

Fig. 4. Weighting functions of the SSH CO_2 channels for the station Dodge City, Kansas on 23 November 1979.

United States. The data sets included synoptic reports and charts, radar summaries, radiosonde observations, DMSP infrared satellite pictures, and colocated SSH infrared and SSM/T microwave sounders data. No additional data sets were obtained because of the enormous amount of effort required in securing the data tapes from the Air Force Global Central, in the processing and analysis of satellite data and in the selection of the colocated radiosonde and synoptic data. The cases selected for comparison purposes are listed in Table 2 in which the satellite pass times represent the actual observation times of the SSH and SSM/T instruments. All 15 cases chosen were ensured to be clear on inspection of satellite infrared pictures and surface reports. Note that the scan times were between 0000Z and 0600Z on the respective dates. In conjunction with the case selection, Fig. 5 depicts the DMSP infrared satellite picture for 30 October 1979, which is from the same spacecraft as the SSH and SSM/T data. The infrared pictures shown in Figs. 6 and 7 for the 23 November 1979 case study had descending node crossing times of 0043Z for the eastern picture and 0224Z for the western picture. A major criterion for the case selection was to have a radiosonde station within the sounder field of view. The satellite pictures have been superimposed with the "footprints" of the microwave sounders and the relative location of the radiosonde stations within them. Below we briefly discuss the synoptic conditions on these two dates.

On 30 October 1979, a surface low pressure center lies off the east coast of the United States near 44^{o}N, 62^{o}W. A cold front extends southward and then west to southern North Carolina, becoming a warm front in northern Georgia to southern Arkansas and into Oklahoma. A dissipating low aloft is portrayed on the 30/0000Z 500 mb chart as a weakness through

Table 2. Selected cases for comparisons between the observed and computed radiances.

Station Name	Satellite Pass Time	Latitude (°N)	Longitude (°W)	Case Type
Jackson Mississippi (MS)	0346 Z 30 Oct 79	32.19	90.05	Clear
Centerville Alabama (AL)	0346 Z 30 Oct 79	32.54	87.15	Clear
Little Rock Arkansas (AR)	3046 Z 30 Oct 79	34.44	92.14	Clear
Monett Missouri (MO)	0347 Z 30 Oct 79	36.53	93.54	Clear
Salem Illinois (IL)	0347 Z 30 Oct 79	38.39	88.58	Clear
Peoria Illinois (IL)	0348 Z 30 Oct 79	40.40	89.41	Clear
Boise Idaho (ID)	0530 Z 30 Oct 79	43.34	116.13	Clear
Desert Rock Nevada (NV)	0529 Z 30 Oct 79	36.60	116.10	Clear
Winnemucca Nevada (NV)	0529 Z 30 Oct 79	40.90	117.80	Clear
Greensboro North Carolina (NC)	0251 Z 23 Nov 79	36.03	79.57	Clear
Chihuahua Mexico (MEX)	0430 Z 23 Nov 79	28.42	106.04	Clear
Del Rio Texas (TX)	0430 Z 23 Nov 79	29.22	100.55	Clear
Dodge City Kansas (KS)	0432 Z 23 Nov 79	37.46	99.58	Clear
Great Falls Montana (MT)	0435 Z 23 Nov 79	47.29	111.22	Clear
Glasgow Montana (MT)	0435 Z 23 Nov 79	48.13	106.37	Clear

Fig. 5. DMSP satellite infrared picture mosaic on 30 October 1979.

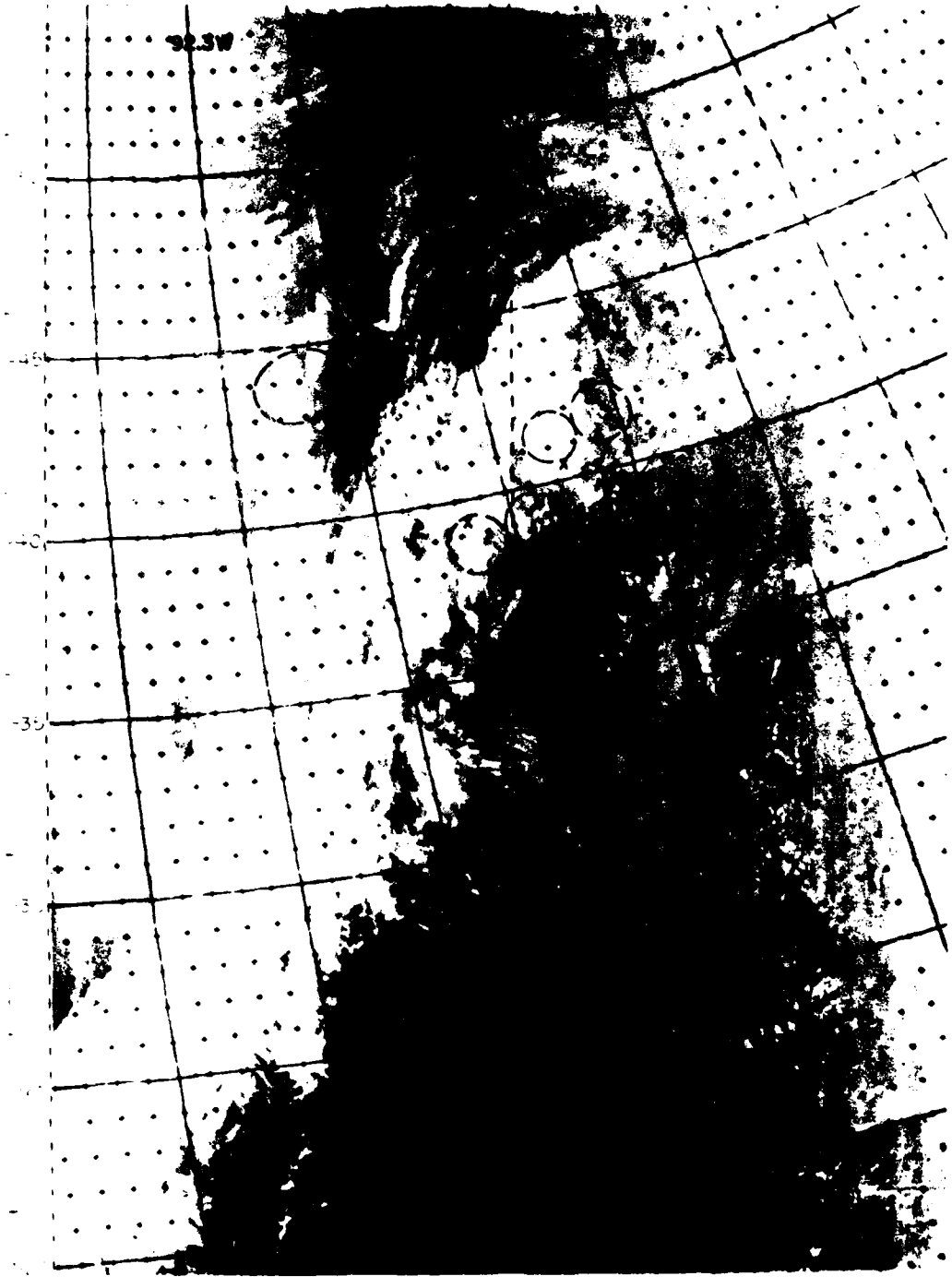

Fig. 6. DMSP satellite infrared picture for the eastern scan on 23 November 1979.

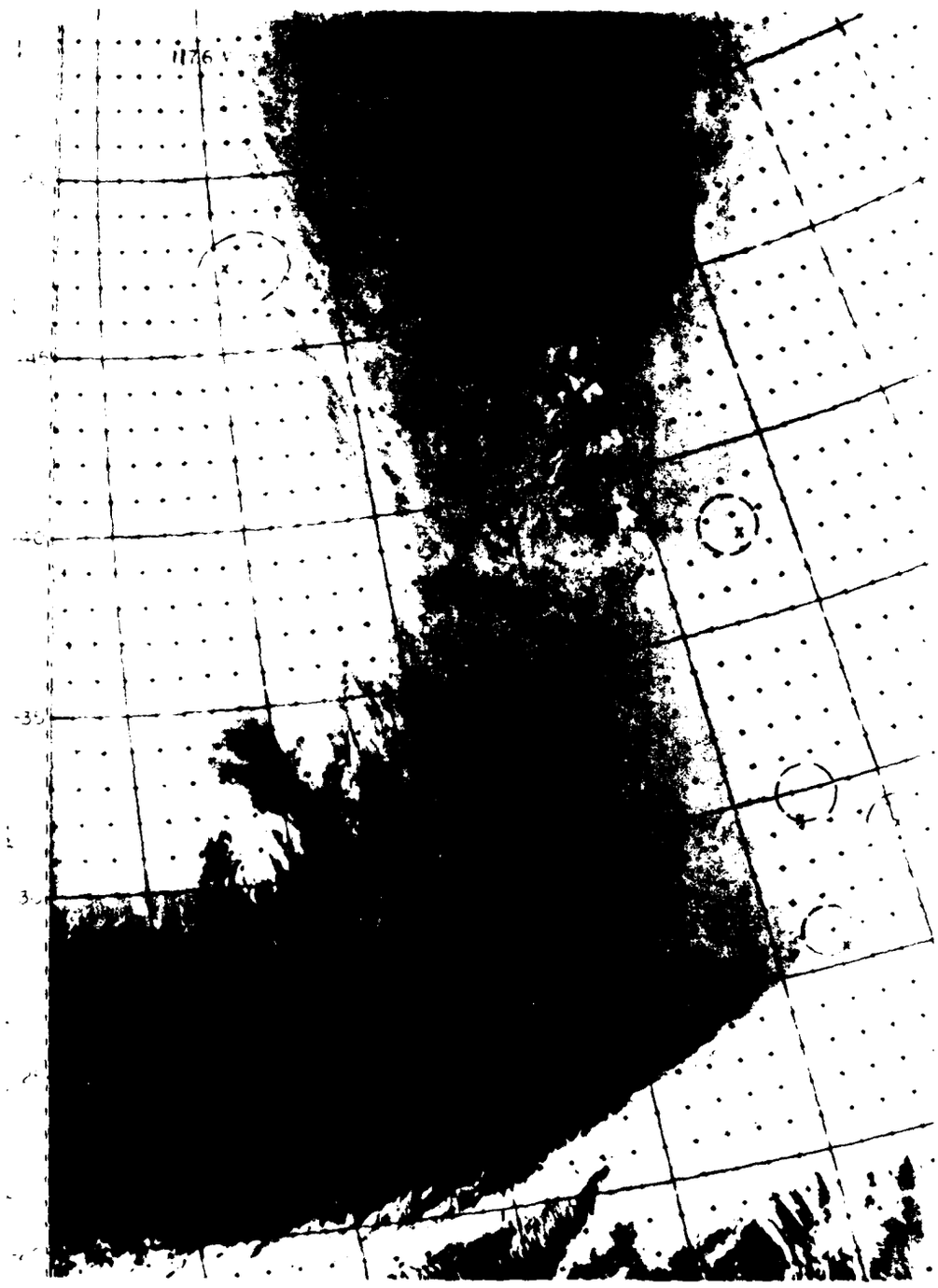

Fig. 7. DMSP satellite infrared picture for the western scan on 23 November 1979.

the Ohio valley.

The dominant feature on the 500 mb map is a storm system that is deepening and moving into northeast Arizona. A surface low pressure center is drawn in southeast New Mexico. Extending northward from this surface low is an inverted trough extending north-northeast to central Minnesota. The 500 mb chart also shows this trough which extends to a low center near 64°N, 107°W. Cloud patterns associated with the southern storm are extensive. A trough at 500 mb just off the west coast of the U.S. supports a surface low drawn near 49°N, 136°W. An occlusion extends south-southeast to a triple point near 43°N, 134°W. This system is moving rapidly and precipitation begins at stations on the Washington and Oregon coasts by 0600Z. The cloud pattern associated with this system appears to be well organized with the cirrus shield already on shore at the satellite pass time.

On 23 November 1979, a dominant 500 mb low pressure center is located in central Minnesota at 23/0000Z. A deep 500 mb trough extends south-southwest to the Texas panhandle and continues southwest into northwest Mexico. On the surface there is a double low system with one low center in south central Minnesota with an occluded front to a second low drawn on the triple point in central lower Michigan. A warm front continues eastward to extreme southern Maine. A cold front extends south through Indiana and into the Gulf of Mexico near New Orleans, Louisiana. Considerable cloudiness accompanies this storm system, extending from the Canadian border across Mexico and into the eastern Pacific. Another system is just off the west coast of the U.S. at 500 mb. The surface map shows a cold front just on the west coast from northern California through western Oregon and Washington. Extensive cloudiness also

accompanies this storm with cloud bands extending along the west coast of the United States. The surface and 500 mb maps can be found in Aufderhaar's thesis (1980) in which a number of cloud and precipitation cases also were chosen in the comparison studies for SST/M channels.

On 30 October 1979, the SSH sounder appeared to be in proper working condition. We have selected nine stations where radiosone and surface reports were available for comparison calculations. On 23 November 1979, however, the SSH data were available only for one station along the satellite pass, i.e., Dodge City, Kansas. The unavailability of SSH data probably was caused by the malfunction of the instrument.

Radiosonde observations (RAOB) under this study were generally available at 0000Z and 1200Z for most of the stations, while the satellite scan times as shown in Table 2 were between 0000Z and 0600Z on the respective dates. Thus, the 0000Z radiosonde observations were considered to be most representative and were used in the calculations. However, surface temperature differences between the times of the satellite pass and radiosonde observation could be quite significant due to radiative cooling effects. Since the surface temperature is normally available hourly from most of the weather stations, we have obtained surface temperature values closest to the satellite pass time in conjunction with the comparison calculations. In addition, temperature corrections in the 70 mb layer nearest the surface, which was considered to be the depth of the radiative cooling, were also carried out by means of a linear interpolation for the temperature difference (between the 0000Z and satellite pass time values) at the surface and zero difference at 70 mb above the surface. The temperature corrections were then subtracted from the RAOB temperatures. Note that the surface temperature difference

between 0000Z and the satellite pass time may be as much as $5^{o}K$.

Upwelling radiances were computed from Eq. (5) using the known temperatures and mixing ratios from RAOB and the transmittance program described previously. A trapezoidal rule was used to perform the integration in which 40 pressure levels were employed with 1000 mb being the lowest layer. For stations whose surface pressures are reported to be less than 1000 mb, the surface and atmospheric terms in Eq. (5) were computed utilizing the reported surface pressure and layers above this pressure level.

There also were cases when the RAOB station did not coincide exactly with the SSH footprint. Because of the horizontal variability of the SSH data, we have devised a distance-weighed method to obtain an average measured radiance from the available SSH data around the RAOB station. This procedure is especially important for wing channels (E5 and E6) which are affected significantly by the surface condition.

Radiosonde observations were available up to 31 km for the clear column case studies with the exception of Chihuahua, Mexico, on 23 November 1979, where the observation was up to 24 km. Where the upper air observation was not available, the spring/fall climatological profile was substituted.

Figure 8 shows results of the comparison of observed and calculated radiances. The average deviations are found to be 2.9, 0.6, 2.7, 4.6, 4.0, and 3.9 for channel 1 through 6, respectively. Generally, comparisons reveal that the calculated radiances are greater than observed values with only few exceptions. For channel 1, because of the lack of the upper air soundings, the discrepancies between the observed data and computed radiances may well be due to the unrealiable temperature

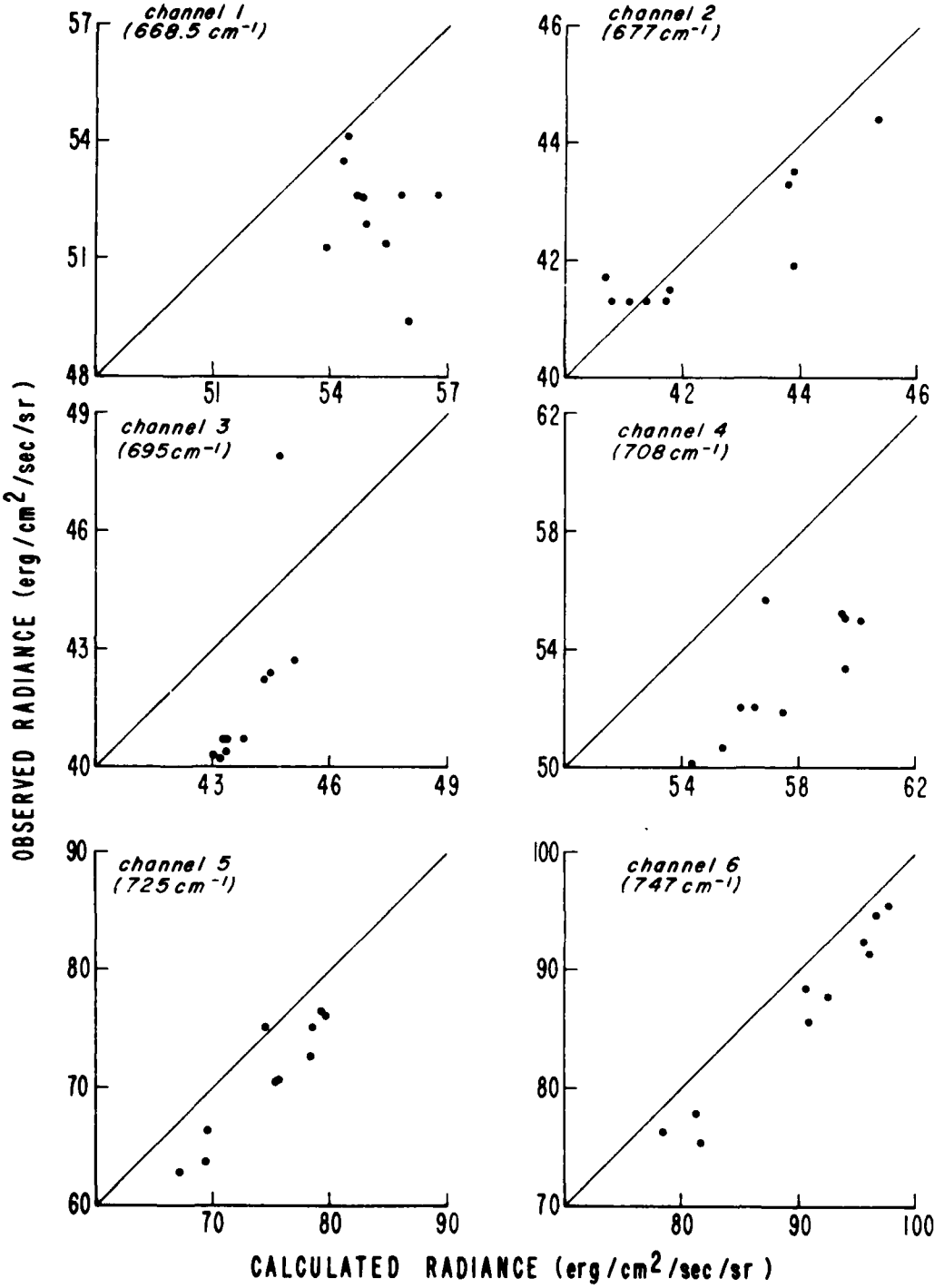

Fig. 8. Calculated and observed clear column radiances for SSH CO_2 channels Scales of the radiances are varied to best reflect each channel.

values from climatology. This argument also may be applied with decreasing significance to channels 2 and 3. We note that for channel 3, there is a point in which the observed data is greater than the computed radiance by as much as 3.2 radiances. This point is for Desert Rock, Nevada, where the available RAOB soundings only were up to about 100 mb. Apparently, the climatological temperature profile used was inapplicable to this station on 30 October 1979. For channel 4, which responds largely to the middle troposphere with little effect from the surface and upper atmosphere, we see a maximum discrepancy in which the calculated values are consistently greater than the observed data. Only for this channel we feel that a definitive conclusion about the discrepancy may be drawn. In Table 3, the exact radiance values for these cases also are given.

At this point, it appears pertinent to discuss the surface effect on the computed radiances in relation to the comparison program. We note from Table 2 that there are three RAOB stations which are over desert areas. Since the height of the standard meteorological instrument shelter is 6 ft., this could cause the actual surface temperature in desert areas to be underestimated by as much as 30°C during the daytime. Assuming that all other physical factors are correct in the context of theoretical calculations, then we would expect that the computed radiance for channels with peak weighting functions close to the surface will be much lower than the observed values. In addition to the surface temperature problem, there are also inherent problems associated with the surface emissivity in the infrared region. As shown in Eg. (5), emissivities in the infrared are normally assumed to be unity. However, for certain minerals and rocks, emissivities could be as low as 0.8-0.9. Although effects of the warmer surface and lower emissivity are opposite and may

Table 3. Comparisons between the observed and computed radiances.

Location		E1	E2	E3	E4	E5	E6
Desert Rock, NV	Calc.	56.0	43.9	44.7	56.9	74.7	91.0
	Obs.	49.4	41.9	47.9	55.7	75.0	85.5
Winnemucca, NV	Calc.	55.8	43.9	44.3	56.1	69.6	81.3
	Obs.	52.6	43.5	42.2	52.0	66.3	77.8
Dodge City, KS	Calc.	55.4	43.8	44.5	54.4	67.2	78.5
	Obs.	51.4	43.3	42.4	50.1	62.9	76.1
Jackson, MO	Calc.	54.4	40.8	43.4	60.2	79.9	97.8
	Obs.	53.5	41.3	40.7	55.0	76.0	95.2
Monett, MO	Calc.	54.7	41.8	43.7	59.6	78.6	95.8
	Obs.	52.6	41.5	40.7	55.1	75.0	92.4
Little Rock, AR	Calc.	54.8	41.4	43.3	59.9	79.3	96.6
	Obs.	52.5	41.3	40.7	55.2	76.1	94.8
Centerville, AL	Calc.	54.5	40.7	43.4	57.2	78.4	96.2
	Obs.	52.1	41.7	40.4	53.3	72.7	91.2
Boise, ID	Calc.	56.7	45.3	45.1	55.4	69.6	81.9
	Obs.	52.6	44.4	42.7	50.7	63.6	75.1
Peoria, IL	Calc.	53.9	41.1	43.2	57.7	75.9	92.7
	Obs.	51.3	41.3	40.2	52.0	70.7	87.7
Salem, IL	Calc.	54.9	41.7	43.0	57.5	75.3	90.9
	Obs.	51.9	41.3	40.3	51.9	70.5	88.3

be compensated for each other, they do pose difficulties in making definitive comparisons between observations and computations for surface channels 5 and 6. However, in view of the greater computed radiances for essentially all the cases, in spite of the colder surface temperatures used in the calculation, the discrepancy between the observed and computed radiances for these two channels appears to be in harmony with the finding for channel 4. It should be noted that not only the desert stations exhibit the general discrepancy for channels 5 and 6, other stations listed in Table 3 also show that the computed radiances for these two channels are greater than the observed values.

2.2 DMSP Block 5D SSM/T Sounder

2.2.1 Characteristics of the SSM/T sounder

As described in subsection 2.1.1, the Passive Microwave Temperature Sounder (SSM/T) is part of the Defense Meteorological Satellite Program (DMSP) Block 5D package. The SSM/T sensor is a cross track scanning radiometer, which acquires data at 32 second intervals and at seven angular positions separated by 12 degrees. The instantaneous field of view ("footprints") of a scan for the SSM/T along the satellite subtrack are shown in Fig. 9. The horizontal resolution is a near circle of 174 km diameter in the nadir direction, while it is an ellipse with a major axis of 304 km and minor axis of approximately 213 km at the maximum scan angle of 36° from nadir.

As shown in Table 4, seven operational frequencies were chosen in the vicinity of a strong oxygen absorption band in the 50-60 GHz region. Figure 10 depicts the weighting functions of the SSM/T channels in the nadir direction for a surface emissivity of 0.97. Channel 1, 50.50 GHz, is a window channel and senses at or near the earth's surface. Channels 2, 3, and 4 (53.20, 54.35, and 54.90 GHz) have weighting functions that peak at increasing heights in the troposphere. The weighting functions of Channels 5, 6 and 7 peak in the stratosphere with Channel 5 peaking highest in the atmosphere near 28 km. The weighting functions result from consideration of atmospheric absorption due to water vapor and molecular oxygen. The weighting functions presented in Fig. 10 also include the transmittance corrections for antenna gain characteristics.

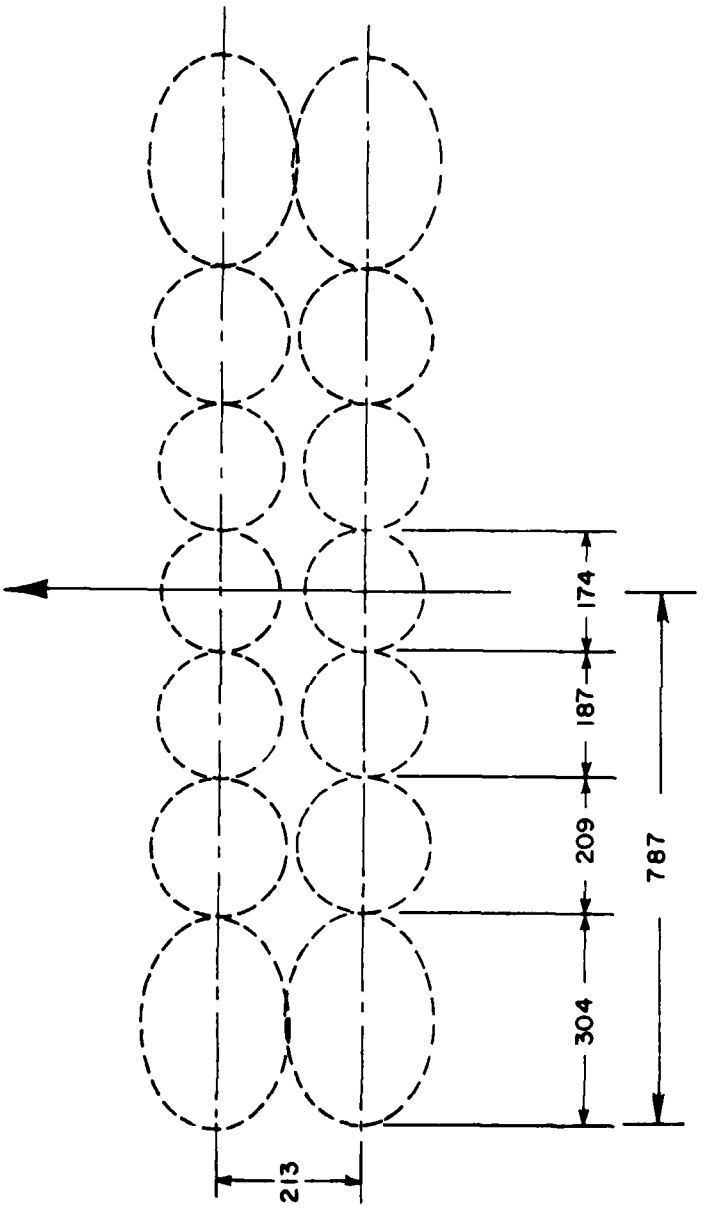

Fig. 9. The scan pattern of SSM/T. Distance Units are in km.

Table 4. Channel parameter design specifications*

Channel	Polarization	Frequency (GHz)	Bandwidth (MHz)	NETD (°K)
1	Principally Horizontal	50.5	400	0.6
2		53.2	400	0.4
3		54.35	400	0.4
4		54.9	400	0.4
5	Orthogonal to Channels 1-4	58.4	115	0.5
6		58.825	400	0.4
7		59.4	250	0.4

*After Rigone and Strogryn (1977).

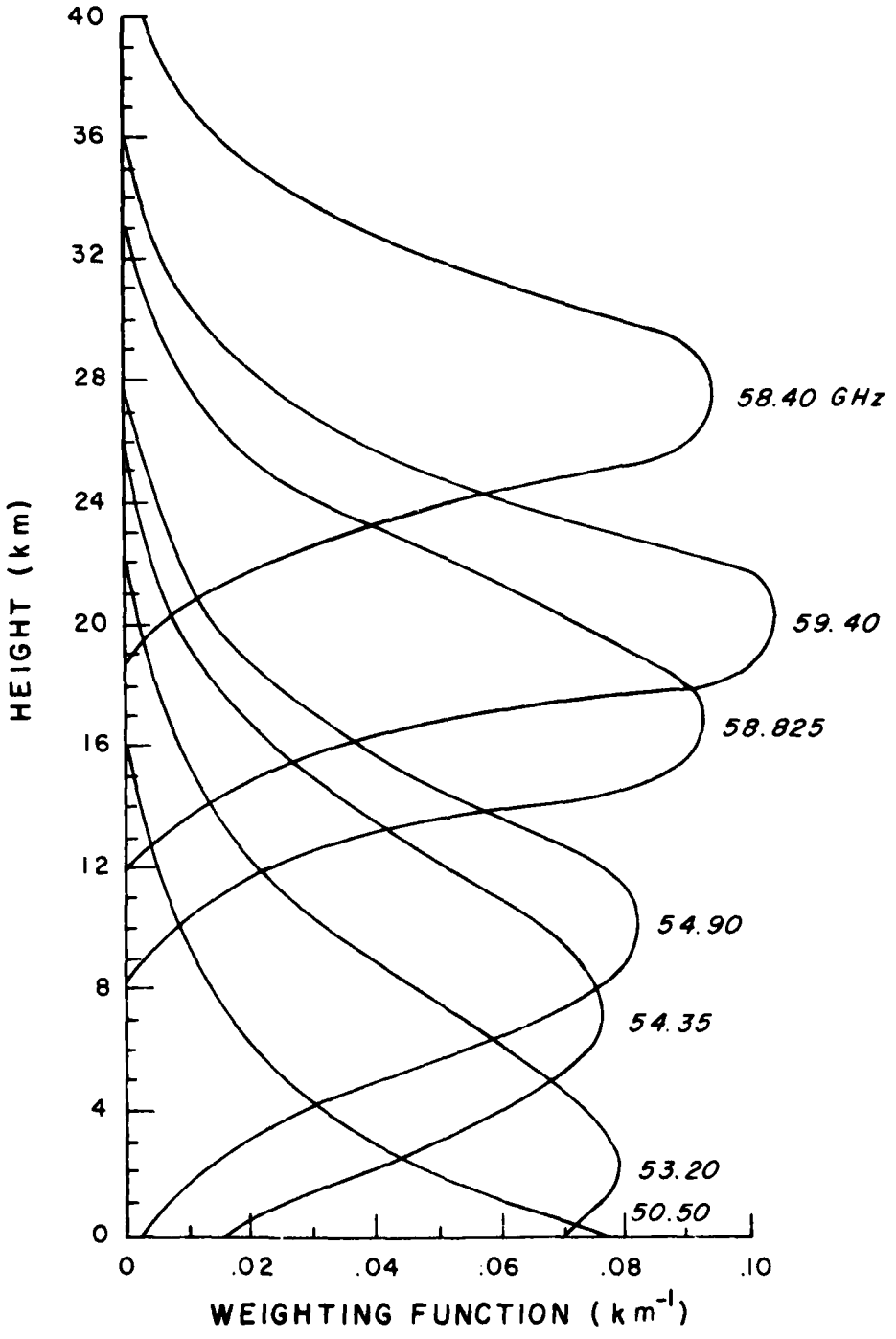

Fig. 10. SSM/T weighting functions (nadir) with antenna gain characteristics included for a surface emissivity of 0.97.

2.2.2 Comparisons between SSM/T data and calculated brightness temperatures

In this subsection we compare the observed data from SSM/T channels and computed brightness temperatures. We shall first present the basic transfer equation in the microwave region and discuss the methods used for the determination of the surface emissivity. We then present the resulting comparisons between the observed data and computed brightness temperatures.

In the microwave region, the brightness temperature in the upwelling direction under the local thermodynamic equilibrium assumption may be expressed by

$$T_B(\tilde{\nu}) = \varepsilon(\tilde{\nu})\, T_s\, \mathcal{T}_{\tilde{\nu}}(P_s) + \int_{P_s}^{0} \left\{1 + [1-\varepsilon(\tilde{\nu})]\left[\frac{\mathcal{T}_{\tilde{\nu}}(P_s)}{\mathcal{T}_{\tilde{\nu}}(p)}\right]^2\right\} \times T(p)\, \frac{\partial \mathcal{T}_{\tilde{\nu}}(p)}{\partial p}\, dp \,, \qquad (7)$$

where $\tilde{\nu}$ denotes the frequency, $\varepsilon_{\tilde{\nu}}$ the surface emissivity, T_s the surface temperature, $\mathcal{T}_{\tilde{\nu}}(p)$ the transmittance with respect to the top of the atmosphere, P_s the surface pressure, and T the atmospheric temperature which is a function of pressure. The first term in Eq. (7) represents the radiation contribution from the surface, while the integral term takes into account atmospheric contributions from the surface to the top of a clear atmosphere in which the reflection contribution from the surface is included in the formula. It is apparent that to simulate the upwelling brightness temperature requires prior knowledge of (1) the atmospheric transmittance of a given frequency, which, in general, is related to the relevant gaseous and temperature profiles, and (2) the surface characteristics, which are described by the surface

temperature and surface emissivity. The transmittance program employed in this study has been described in a previous AFGL report by Liou et al. (1979) and so we shall not give further discussion here. However, the surface emissivity and surface temperature are important factors in the brightness temperature computation and require some analysis.

It is well-known that one of the major problems in microwave sounding over land areas is the uncertainty of the surface emissivity. Gloersen, et al. (1972) have presented microwave emissivity values ranging from approximately 0.80 over wet bare soil to 0.98 over a uniformly vegetated surface. This background variability coupled with atmospheric uncertainties (e.g., clouds and precipitation) considerably complicate the remote sensing effort. In a clear atmosphere the radiative transfer problem is somewhat simplified and the surface emissivity may be estimated by an objective scheme. Two such schemes were investigated in conjunction with the theoretical computations.

The first method involves solving the radiative transfer equation for the surface emissivity using the window frequency of 50.50 GHz(ν_1). This frequency's weighting function peaks at or near the surface and we may construe that the bulk of the energy received by an observer at the top of the atmosphere at this frequency had its origin at the surface. For simplicity of analyses, we define the following terms:

$$
\begin{aligned}
a_1 &= \mathcal{T}_{\tilde{\nu}_1}(p_s) \ , \\
b_1 &= \int_{p_s}^{0} T(p) \, \frac{\partial \mathcal{T}_{\tilde{\nu}}(p)}{\partial p} \, dp \ , \\
c_1 &= \int_{p_s}^{0} T(p) \left[\frac{\mathcal{T}_{\tilde{\nu}}(p_s)}{\mathcal{T}_{\tilde{\nu}}(p)} \right]^2 \frac{\partial \mathcal{T}_{\tilde{\nu}}(p)}{\partial p} \, dp \ .
\end{aligned}
\tag{8}
$$

Substituting Eq. (8) into Eq. (7) and solving for ε, we find

$$\varepsilon(\tilde{\nu}_1) = \frac{T_B(\tilde{\nu}_1) - b_1 - c_1}{T_S\, a_1 - c_1} \tag{9}$$

For the clear column case studies, the atmosphere radiosonde profiles may be used to generate the transmission function, and the surface temperature averaged over the satellite "footprint" may be estimated from the synoptic reports. Consequently, Eq. (9) may be used to solve for the 50.50 GHz surface emissivity from the observed brightness temperature $T_B(\tilde{\nu}_1)$. Moreover, it has been generally found that the emissivity does not have appreciable change in value between 50.50 and 59.40 GHz (Gloersen, et al., 1972). Thus, the 50.50 GHz value may be employed in brightness temperature calculations for the remaining channels.

The second method involves an attempt to derive both the surface emissivity and surface temperature from channel 1 (50.50 GHz) and channel 2 (53.20 GHz), the wing channel whose weighting function peak was nearest the surface. We divide the transfer equation for 50.50 GHz by that for 53.20 GHz ($\tilde{\nu}_2$) to give

$$\frac{\varepsilon(\tilde{\nu}_1)\, T_S\, a_1}{\varepsilon(\tilde{\nu}_2)\, T_S\, a_2} = \frac{T_B(\tilde{\nu}_1) - b_1 - c_1 + \varepsilon(\tilde{\nu}_1)\, c_1}{T_B(\tilde{\nu}_2) - b_2 - c_2 + \varepsilon(\tilde{\nu}_2)\, c_2}\ , \tag{10}$$

where the subscript 1 refers to 50.50 GHz and 2 refers to 53.20 GHz. Since $\varepsilon(\tilde{\nu}_1) \approx \varepsilon(\tilde{\nu}_2)$, we find

$$\varepsilon(\tilde{\nu}_1) = \frac{T_B(\tilde{\nu}_1) - b_1 - c_1 - (a_1/a_2)[T_B(\tilde{\nu}_2) - b_2 - c_2]}{(a_1/a_2)\, c_2 - c_1}\ . \tag{11}$$

Subsequently, the surface temperature may be obtained from Eq. (9).

Surface temperature and emissivity values generated by methods 1 and 2 are presented in Table 5. The emissivities calculated by method 1 seem to be more in agreement with published values (Gloerson, et al., 1972) for the different types of ground surfaces than those of method 2. Therefore, the emissivities of method 1 were used for the clear column calculations of the remaining SSM/T frequencies.

Figure 11 shows comparisons between the SSM/T data and computed brightness temperatures. Note that the 50.50 GHz diagram is not shown since the calculated and observed values will match extactly for this frequency when method 1 is used. At 53.20 GHz there is generally agreement between the calculated and observed brightness temperatures, with most of the calculations slightly underestimating the observed values. The brightness temperature at 53.20 GHz is significantly affected by the surface. In addition, we have pointed out previously that the observed surface temperature is normally smaller than the true surface temperature. These facts may provide a possible explanation for calculated brightness temperatures being lower than the observed data at this surface channel.

In reference to Fig. 10, it is seen that the weighting function for 58.4 GHz has the heighest peak at about 28 km. Since the soundings are normally available up to about 30 km, the calculated brightness temperatures are affected significantly by the climatological temperature profile used in the calculations. Because of the uncertainty of utilizing the climatology, the comparisons shown in Fig. 11 for this channel, where the calculated values are slightly smaller than observed data, may not be conclusive.

Table 5. Generated emissivities and surface temperatures.

Station	Method 1		Method 2	
	ε	T_s^1(°K)	ε	T_s^2(°K)
Jackson, MS	.954	289.8	.890	303.4
Centerville, AL	.949	289.8	.895	301.1
Little Rock, AK	.958	287.1	.901	299.4
Monett, MO	.971	287.1	.902	301.9
Salem, IL	.969	282.1	.873	302.5
Peoria, IL	.940	285.9	.894	295.9
Dodge City, KS	.933	273.2	.896	281.3
Del Rio, TX	.924	284.6	.905	288.9
Great Falls, MT	.908	275.9	.933	270.6
Glasgow, MT	.902	281.4	.927	275.7
Greensboro, NC	.935	290.9	.873	305.2
Chihuahua, MEX	.912	280.6	.948	272.4
Desert Rock, NV	.900	281.5	.814	307.5
Boise, ID	.906	273.2	.921	270.2

[1]Derived from the surface report.

[2]Computed from method 2.

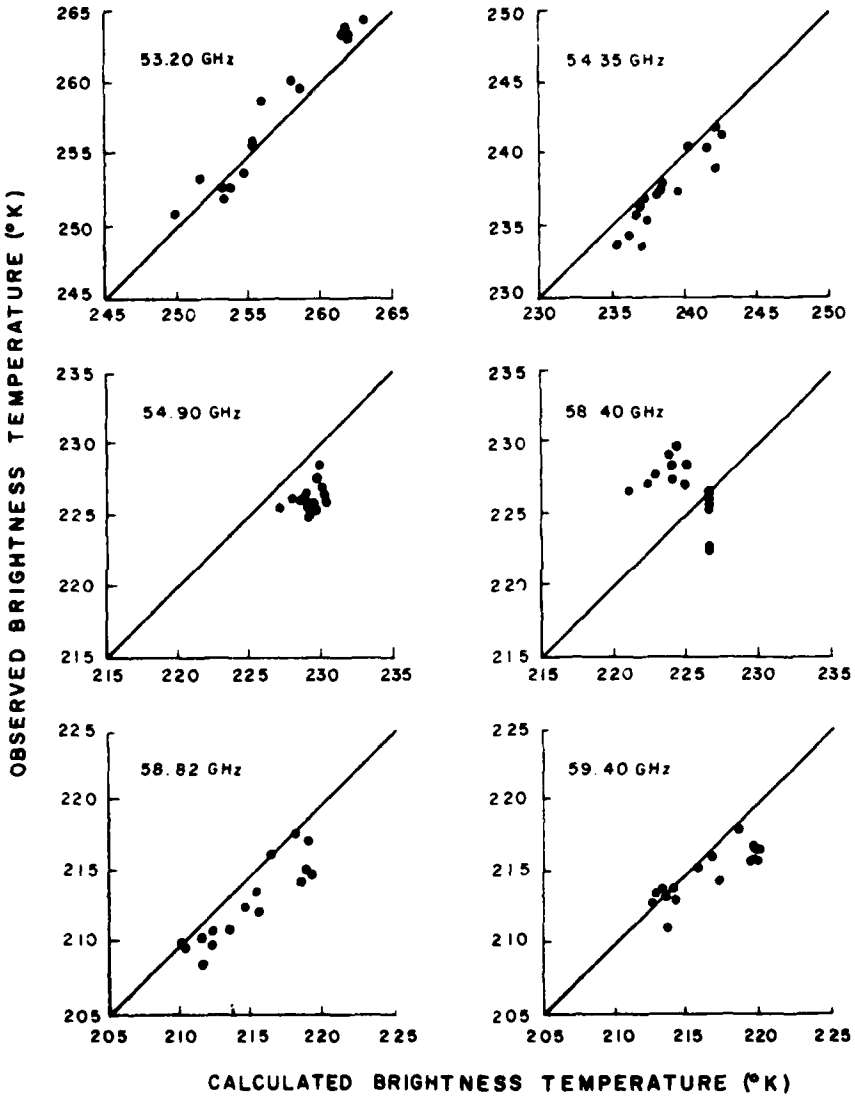

Fig. 11. Calculated and observed clear column brightness temperatures for SSM/T channels. Scales of the brightness temperatures are varied to best reflect each channel.

The peaks of the weighting functions for 59.40, 58.82, 54.35 and 54.90 GHz shown in Fig. 10 are well below 30 km where the temperature profile is known through RAOB. Moreover, from transmittance calculations, we find that atmospheric transmittances for 59.4, 58.82, 54.35, and 54.90 GHz are approximately 0.000, 0.000, 0.023 and 0.003, respectively. Thus, the brightness temperatures at these four frequencies are not appreciably affected by the surface but are mainly due to the contribution of the atmosphere. In Fig. 11 we see that the calculated brightness temperatures at these four channels overestimate the observations with 58.82 GHz by a larger amount in the average. This find appears to be in agreement with the infrared calculations reported in subsection 2.1.2.

SECTION 3

COMPARISON BETWEEN OBSERVED NIMBUS 6 DATA AND CALCULATED RADIANCES

In parallel to the comparison program using the DMSP data set described in Section 2 and in order to have an independent investigation and cross-check concerning the discrepancies between the observed and computed radiances, we have also carried out a smaller comparison program employing the Nimbus 6 HIRS and SCAMS data. In this conjunction, we have examined more than 20 weather stations over the United States and their sounding reports for 25 August 1975 during which both the SCAMS and HIRS data are available. However, we have eliminated a number of stations either because the station is too close to water and sea surfaces or because the station does not have adequate upper air soundings. These elimination processes leave us with only 12 stations for infrared computations and 10 stations for microwave calculations in the comparison program. Moreover, as pointed out previously, radiosonde data are normally available up to about 10 mb or about 16 km or so. Because of the unavailability of soundings above about 10 mb, again a standard climatological profile is assumed for the temperature and water vapor concentration. The sources of transmittances employed in this investigation and the characteristics of HIRS and SCAM channels have been well documented in the papers by Feddes and Liou (1978), Liou and Duff (1979), and Liou et al. (1980).

Figure 12 shows comparisons between the calculated and observed radiances for the 15 μm CO_2 and 11 μm window channels. Near the center of the band (channel 1), the observed radiances show a great variety of values ranging from 45 to 75 erg sec^{-1} cm^{-2} sr^{-1} $/cm^{-1}$, revealing strong horizontal temperature gradients in the upper atmosphere between these stations. However, the computed values vary only slightly because of the use of the standard atmospheric temperature for all the stations. For channel 2 the influence of the unreliable upper air soundings still can be noted. For channels 3-5, with weighting functions peaking at levels progressively close to the surface, we find that the calculated radiances are generally higher than the observed data for three channels with standard deviations of 1.35, 1.35, and 1.61 radiances, respectively. The overestimations of the calculated values in these cases are in general agreement with results presented in subsection 2.1.2. We note that surface contributions for these three channels are nominal and their upwelling radiances are mainly contributed from the atmosphere.

Comparisons for channels 6 and 7 in the wing of the 15 μm CO_2 band also indicate significant discrepancies between the calculated and observed radiances with calculations overestimating observed data by 2.85 and 3.87 radiances in the average, respectively. We wish to point out here in accord with the discussions in subsection 2.1.2 that upwelling radiances for these two channels are affected appreciably by the surface condition. And in spite of the colder temperatures employed in the calculation, the computed radiances are found to be generally greater than the observed values. For the 11 μm window channel, the computed radiances are generally much lower than the observed data.

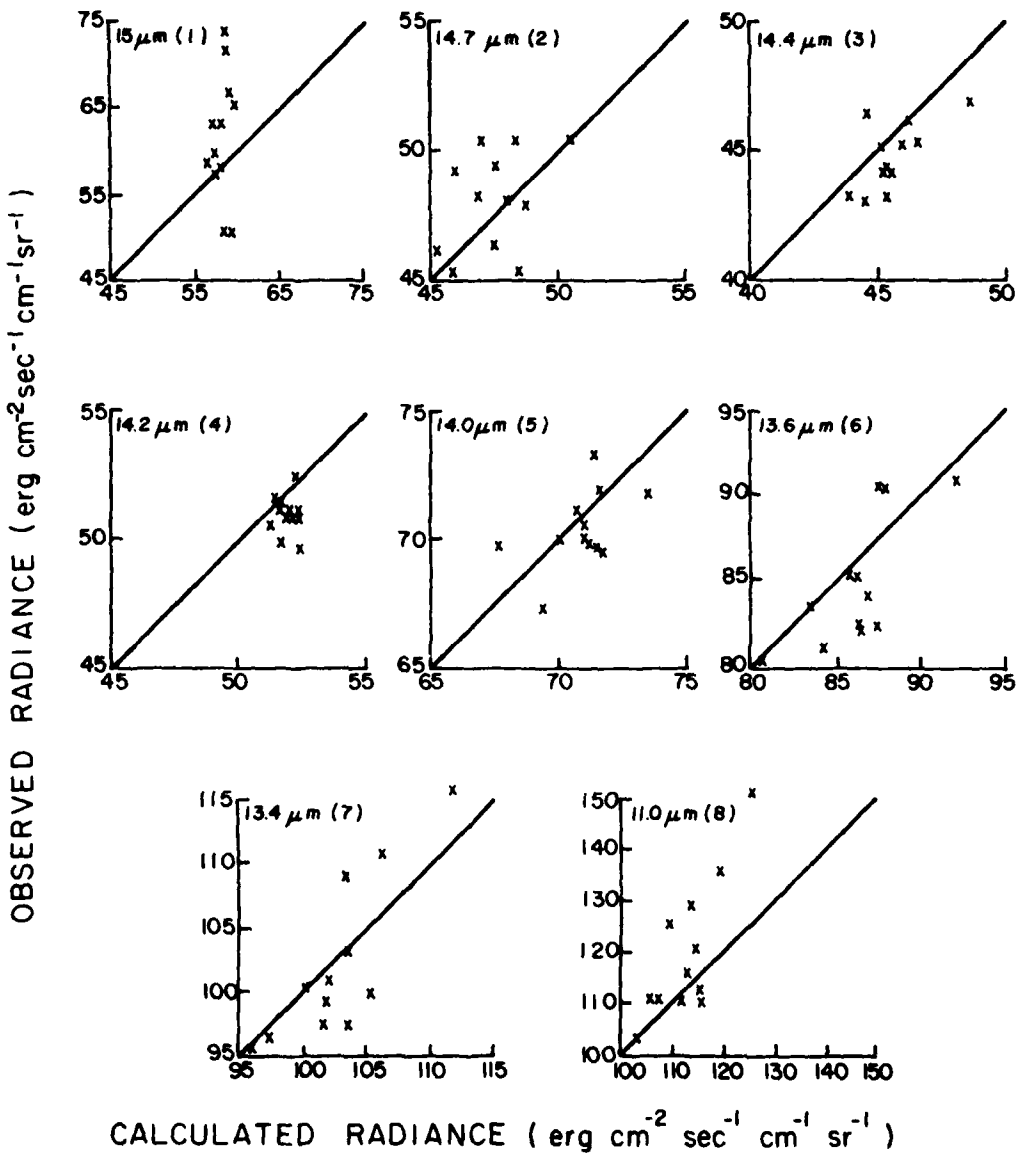

Fig. 12. Calculated and observed clear column radiances for HIRS 15 μm CO_2 and window channels. Scales of the radiances are varied to best reflect each channel.

The lower computed values may be explained by the colder observed surface temperatures used in the computation. In addition, we also note that not only the temperature field but also the water vapor concentration affects the upwelling radiance for this channel. The uncertainties in the observed surface temperature and mixing ratio hamper an adequate physical explanation for the discrepancy in this case.

In the microwave transfer calculation, the surface emissivity plays a very significant role in brightness temperature values as pointed out in subsection 2.2.2. The SCAMS instrument consists of one window channel at 31.65 GHz, one water vapor channel at 22.235 GHz, and three oxygen channels at 52.85, 53.85, and 55.45 GHz. Because of the diversity of the sounding frequencies, we have not attempted to derive the surface emissivity from the observed data in conjunction with the comparison program. But rather, we have assumed known emissivity values for the respective frequencies in dry surface conditions based on the report by Gloersen et al. (1972).

For channel 1 at 22.235 GHz, a surface emissivity of 0.95 for dry surfaces is used according to Gloersen et al. Resulting comparisons shown in Fig. 13 reveal fairly good agreement between the computed and observed brightness temperature. The standard deviation of calculated values from observed brightness temperatures in this case is 1.28°K. For channel 2 at 31.65 GHz, we use a surface emissivity of 0.96 according to the aforementioned report. A similar comparison as in channel 1 is shown with a standard deviation of 1.57°K. A surface emissivity of 0.97 is utilized for the oxygen band again based on the report by Gloersen et al. The differences between observed and computed values

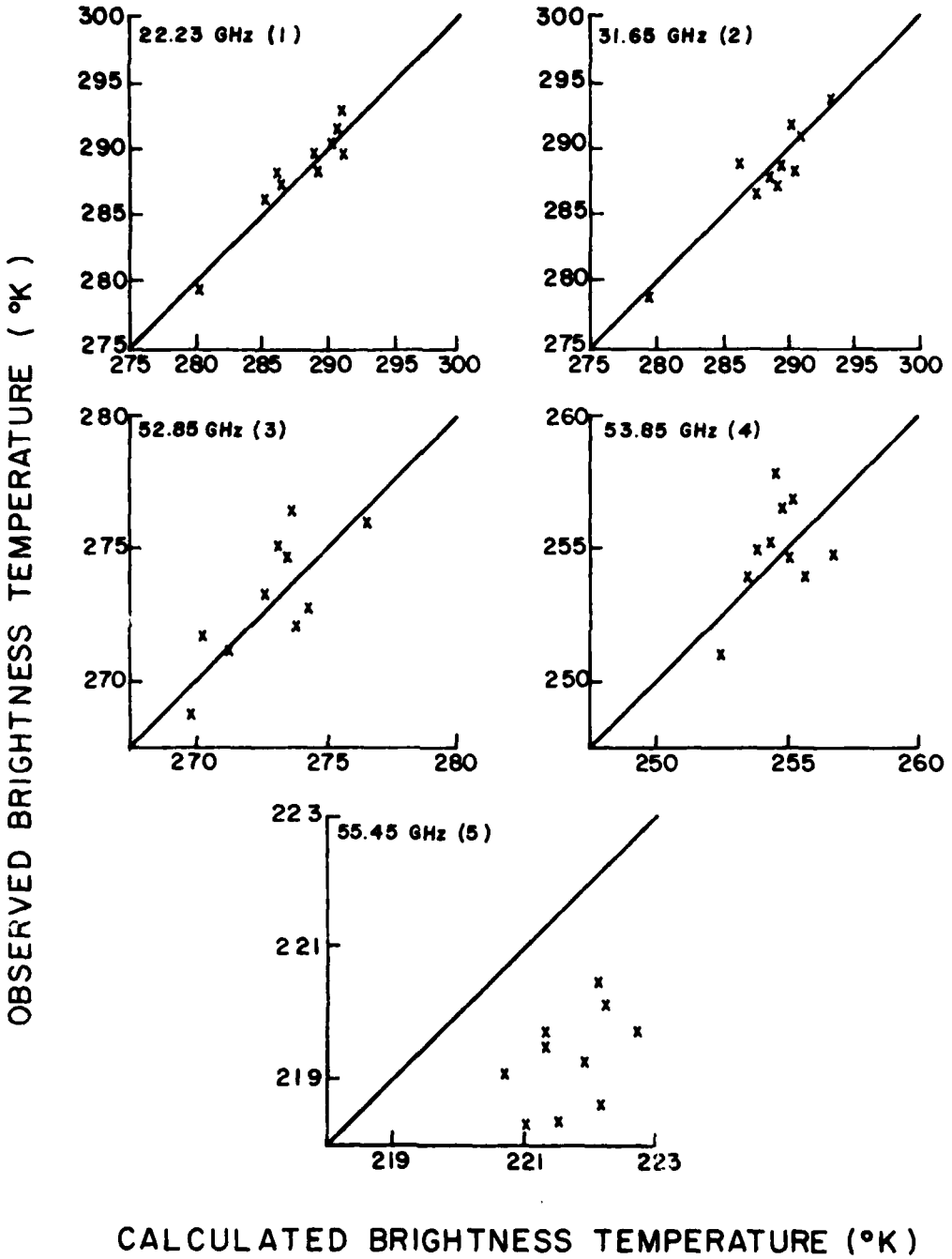

Fig. 13. Calculated and observed clear column brightness temperatures for SCAMS channels. Scales of the brightness temperatures are varied to best reflect each channel.

for channels 3 and 4 are similar to those for channels 1 and 2 with respective standard deviations of 1.59 and 1.78. In the center of the oxygen band (channel 5), we find that the computed values are consistently higher than the observed data. These discrepancies may be attributed to the fact that the weighting function peak of this channel is above about 10 mb where no observed temperatures are available from the radiosonde. Apparently, the standard temperature profile assumed could be higher than the actual profiles on 25 August 1975. Except channel 5 at 55.45 GHz, we do not see a consistent discrepancy between the computed and observed brightness temperatures for channels 3 and 4 at 52.85 and 53.85 GHz. Note that the observed surface temperatures used in the calculation, as pointed out repeatedly in the earlier subsections, were underestimated. Moreover, it should be emphasized that the surface emissivities used in this particular study were not obtained from an objective means but were assumed values for all stations. In any event, the surface emissivity problem in the microwave region introduces extreme difficulties in making appropriate comparisons between observations and computations. It would be desirable for the purpose of investigating the possible discrepancy between the observed and computed brightness temperatures to develop a retrieval scheme from the available sounding channels for the inference of the surface emissivity.

SECTION 4

CONCLUSIONS

In this report, we have carried out comparison programs involving the computed radiances and brightness temperatures, utilizing the observed temperature and mixing ratio profiles from radiosonde, and the observed data from DMSP and Nimbus 6 satellites. Comparisons have been done for carefully selected stations where colocated satellite data and conventional meteorological observations are both available. We have first presented comparison results using the DMSP and SSM/T data in which the characteristics of these two sensors have been described in some details. We subsequently discuss a parallel comparison program utilizing the Nimbus 6 HIRS and SCAMS data to independently examine the probable discrepancies between computations employing the conventional transfer equation and satellite observations. Below we summarize highlights of these investigations.

(1) For the SSH 15 μm CO_2 temperature channels, appreciable discrepancies between computations and observations are shown for channels 3-6 whose weighting function peaks are below the tropopause. Computations generally exceed the measured radiances with channel 4 showing the largest differences which is affected insignificantly by the surface and upper air soundings. This conclusion seems to be in general agreement with the findings presented by McClatchey (1976).

(2) For the SSM/T temperature channels, we also find that computations overestimate the observed values for 54.90 and 54.35 GHz

which are influenced little by the surface and upper air soundings. This conclusion is subject to the reliability of the surface emissivity determination from the surface channel (50.50 GHz).

(3) Utilizing an independent data set from the Nimbus 6 HIRS 15 μm CO_2 channels, the computed radiances are found to be generally higher than the observed data for channels whose weighting functions peak below the tropopause. This find is in agreement with (1). However, due to the uncertainty in the assumed surface emissivity, the SCAMS data and computed brightness temperatures do not show consistent discrepancies.

(4) Because of the unavailability of the upper air soundings, no definitive conclusion could be made for channels whose weighting function peaks are above about 31 km.

In view of these finds, there appears to be definitive discrepancies between the computations and observed radiances, with the computations overestimating the measured data, at least in the infrared frequencies whose upwelling energies arise primarily from the atmosphere. It is likely that the overestimation in the theoretical computation may be due to the incorrect account of the Planck source function in the integral solution of the fundamental transfer equation. Following these investigations, it seems logical to recommend that a carefully designed field experiment, involving simultaneous and colocated infrared radiance observations in the 15 μm CO_2 frequencies and temperature and mixing ratio measurements, be carried out to further examine the quantitative validity of the radiative transfer equation which has been basic to the sounding of the temperature profile from orbiting meteorological satellites.

REFERENCES

Aufderhaar, G. C., 1980: A cylindrical cloud model for microwave and infrared radiative transfer: Applications to DMSP microwave sounders. Ph.D. dissertation, Department of Meteorology, University of Utah, Salt Lake City, Utah.

Barnes Engineering Company, 1976: Technical report prepared for SAMSO, 2413-TA-015.

Feddes, R. G. and K. N. Liou, 1973: Atmospheric ice and water content derived from parameterization of Nimbus 6 High Resolution Infrared Sounder data. J. Appl. Meteor., 17, 536-551.

Gloersen, P., T. Wilheit, and T. Schmugge, 1972: Microwave emission measurement of sea surface roughness, soil moistures, and sea ice structure. Fourth Annual Earth Resources Program Review, NASA Programs, Goddard Space Flight Center, Greenbelt, Maryland, 8-1 - 8-19.

Liou, K. N., 1980: An Introduction to Atmospheric Radiation. Academic Press (International Geophysics Series No. 26), New York, 392 pp.

Liou, K. N. and A. D. Duff, 1979: Atmospheric liquid water content derived from parameterization of Nimbus 6 Scanning Microwave Spectrometer data. J. Appl. Meteor., 18, 99-103.

Liou, K. N., H. Y. Yeh, F. M. Chen, K. Hutchison, and E. Astling, 1980: Development of infrared and microwave techniques for cloud parameter inference from satellite imagery and sounder data. Scientific report, Air Force Geophysics Laboratory, Hanscom AFB, Massachusetts.

McClatchey, R. A., 1976: Satellite temperature sounding of the atmosphere: Ground truth analysis. AFGL-TR-76-0279, Air Force Geophysics Laboratory, Hanscom AFB, Massachusetts. AD A038236.

Rigone, J. L. and A. P. Strogryn, 1977: Data processing for the DMSP Microwave Radiometer System. 11th Inter. Symp. Remote Sensing of the Environment, Univ. of Michigan, pp. 1599-1608.

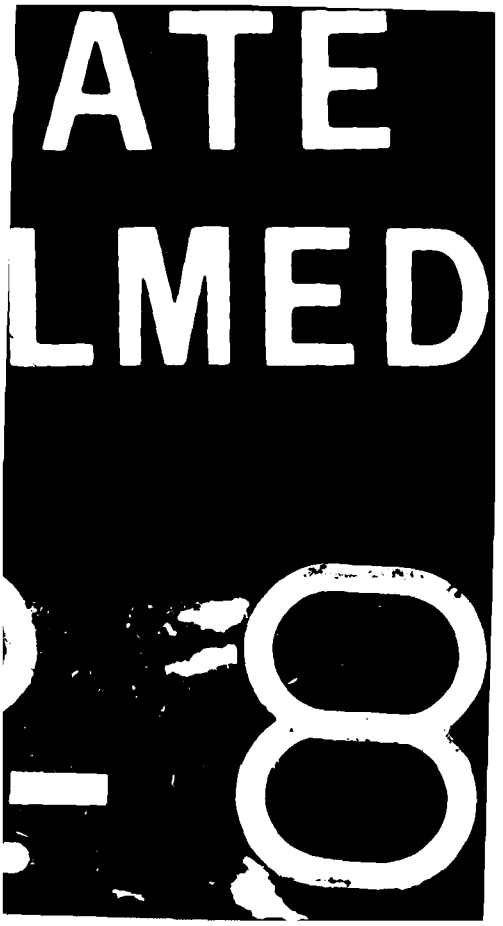
ATE
LMED
8